Laboratory simulation of ionospheric instabilities*

Y. C. Saxena
Institute for Plasma Research, Bhat, Gandhinagar 382 424, India

Results of laboratory experiments simulating conditions of the ionospheric plasma are described. Spectral and dispersion characteristics of the instabilities are measured and compared with *in situ* measurements in ionospheric plasma. Results indicate an important role of these instabilities in the generation of plasma irregularities.

THE equatorial ionosphere exhibits strongly field-aligned plasma density irregularities over a wide range of scale sizes[1]. These irregularities arise from plasma instabilities due to specific geometries and plasma characteristics in different regions of the ionosphere. The equatorial electrojet in the E-region is characterized by a weakly ionized plasma embedded in a horizontal magnetic field and having magnetized electrons (the electron gyro frequency, $\Omega_e \gg \nu_{en}$, the electron–neutral collision frequency), collisional ions (the ion gyro frequency, $\Omega_i \leq \nu_{in}$, the ion–neutral collision frequency), and vertical density gradients parallel to the polarization electric field. The density irregularities in this region have been observed by radar[2] and rocket-borne *in situ*[3] experiments. Both Farley–Buneman[4] instability and the density-gradient-driven gradient drift instability, or the cross-field[5] instability, have been known to be responsible for these density irregularities. The equatorial spread-F[6] (ESF) is another ionospheric phenomenon involving a very broad range of highly field-aligned irregularities. The electrostatic fluctuations associated with the ESF arise due to the special geometry of the bottom side of the F-region plasma, with density gradients (∇n) antiparallel to the gravity (**g**) and perpendicular to the magnetic field, together with the fact that the plasma is weakly ionized with magnetized electrons and ions ($\nu_{en} \ll \Omega_e$; $\nu_{in} \ll \Omega_i$). Both Rayleigh–Taylor (RT) and the drift wave instabilities are known to play an important role in the ESF[7].

In what follows, we summarize the results of our laboratory experiments simulating the plasma processes responsible for the production of instabilities in the equatorial ionospheric plasma. The experiments reported do not represent an exact scaled simulation of the plasma parameters of the ionospheric plasma to the laboratory plasma but an attempt to produce these instabilities in the laboratory plasma with a view to study their spectral and dispersion characteristics in the nonlinear regime.

Experiments on F-region instabilities

The nighttime equatorial F-region plasma density profiles[8] indicate two distinct regions: region I corresponding to the bottom side of the density peak, having the geometry described as above, and region II above

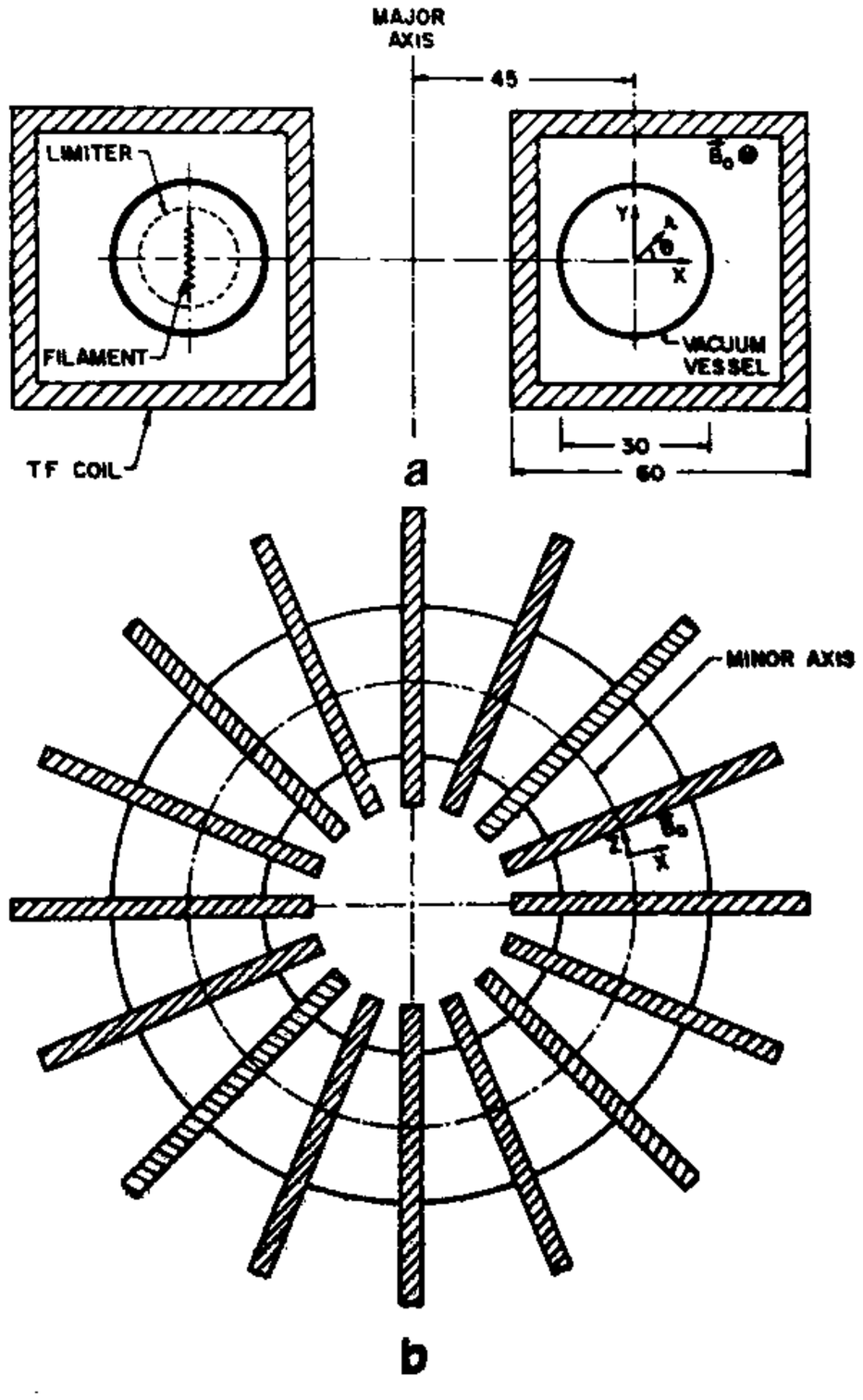

Figure 1. Schematic diagram of the experimental device BETA. *a*, Vertical section showing toroidal field coils, vacuum vessel, limiter and filaments along with the major and minor axes and the coordinates used in the text. *b*, Top view of the device.

*Text of the talk delivered at the Symposium on Interactive Processes in the Near Earth Environment at the 58th Annual Meeting of the Indian Academy of Sciences, November 6–9, 1992, Physical Research Laboratory, Ahmedabad, India.

the peak density, with ∇n parallel to **g**. We have recently carried out, for the first time, experiments on low-frequency instabilities in laboratory plasma simulating essential features of the nighttime equatorial F-region of the ionosphere[9]. The gravity is simulated by the curvature of the magnetic field. In one of these experiments (hereafter referred to as type-I experiment), conditions on the bottom side of the nighttime F-region are simulated with **g** antiparallel to ∇n. In another experiment (hereafter referred to as type-II experiment), the plasma produced has both the regions, i.e. region I, where ∇n is antiparallel to **g**, and region II, where ∇n is parallel to **g**.

These experiments were carried out in the toroidal plasma device BETA[10], shown schematically in Figure 1 and consisting of a torus having a major radius of 45 cm and a minor radius of 15 cm placed in a pure toroidal field, generated by means of 16 coils placed around the torus. A maximum toroidal magnetic field of 1 kG could be produced for time up to 1.2 s with a DC power supply. The system was pumped down by a diffusion pump to a base pressure of 10^{-6} torr. The plasma was produced in argon gas at $\approx 10^{-4}$ torr by striking a discharge between an incandescent tungsten filament acting as a cathode and the vessel wall acting as an anode. A grounded limiter, 9 cm in radius, was used to short-circuit the charge separation electric field due to the curvature of the toroidal magnetic field.

Radially movable cylindrical Langmuir probes were used to measure the equilibrium profiles of plasma density, the floating potential and the electron temperature, and to record the density and the floating-potential fluctuations. The data were acquired at different radial and azimuthal locations using an eight-channel CAMAC-based data acquisition system with simultaneous sampling and a sampling time of 25 μs for each channel. The data were analysed using the standard FFT-based spectral analysis techniques[11] for obtaining dispersion and spectral characteristics. The frequency spectrum exhibits turbulence for values of magnetic field above 600 G. In a turbulent medium there does not exist a deterministic relationship between frequency and wavenumber. In order to estimate the wavenumber spectra for the observed fluctuations, the data from a pair of probes were analysed using a technique outlined by Beall *et al.*[12].

Two sets of experiments were carried out. In these experiments, the effect of gravity was simulated by a curved magnetic field with $g = C_s^2 / R$, where C_s is the ion acoustic speed and R is the major radius of the system. The effect of gravitational field for $\nu_{in}/\Omega_i \ll 1$ is relatively strong with $E_0/B < g/\nu_{in}$.

Type-I experiments

In these experiments the filament was located near the inner wall of the vacuum vessel to simulate the profile for the bottom side of the F-region and the measurements were made at a toroidal location 180° away from the location of the filament. The observed density and floating-potential profiles at one azimuthal location in a plane perpendicular to the toroidal magnetic field are shown in Figure 2. The plasma peak density is $\sim 10^{11}$ cm^{-3}, and the electron temperature in the region where the experiment is performed is ~4 eV. The ion temperature $T_i = 0.23 \pm 0.06$ eV as measured by an ion-collecting probe. Typically, the experimental region has an electric field of $\simeq 0.7$–1.0 Vcm^{-1}. It is clear from Figure 2 that ∇n is antiparallel to **g** all through the plasma cross-section.

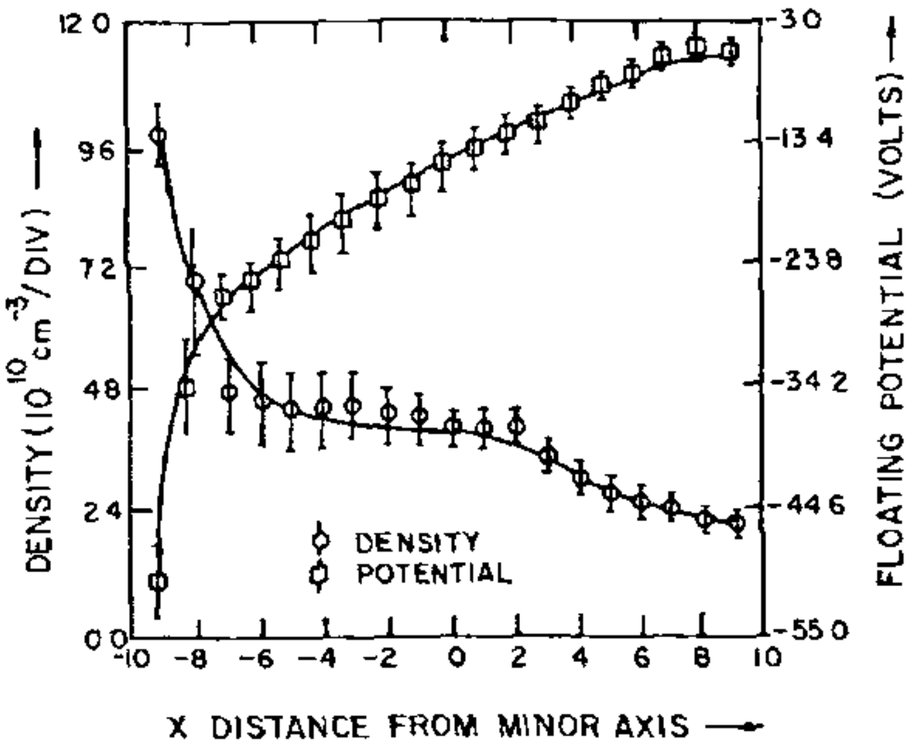

Figure 2. Variation of the plasma density and the floating potential as a function of the distance x from the minor axis at one toroidal location in type-I experiments.

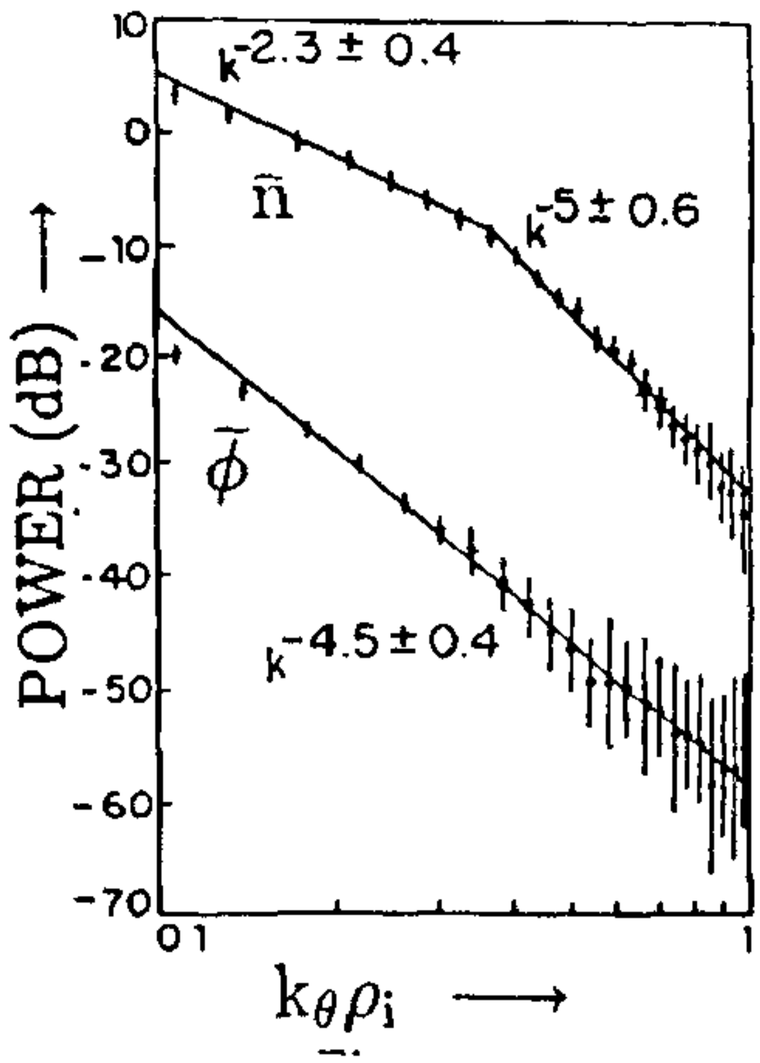

Figure 3. Wavenumber spectra for density and potential fluctuations in type-I experiments.

Strong density and potential fluctuations having frequencies in the range of $\omega < \Omega_i, \nu_{en}$, $\langle \tilde{n}/n_0 \rangle_{rms} \approx$ 20–40% for different values of the magnetic field, and $\langle \tilde{n}/n_0 \rangle_{rms} \approx \langle e\tilde{\phi}/T_e \rangle_{rms}$ are observed. The measurements of radial and parallel wave numbers indicate that the waves have long wavelength in the radial and parallel directions and propagate mainly in the azimuthal direction.

The wavenumber spectra for density and potential fluctuations for $\nu_{in}/\Omega_i \sim 0.1$ are shown in Figure 3. The spectrum for density fluctuations exhibits a break at $k_\theta \rho_i = 0.3$. The spectrum follows a power law, $S(k) \propto k^n$, with the index $n \sim -2.5$ for $k_\theta \rho_i < 0.3$ and -4.5 for $k_\theta \rho_i > 0.3$. The potential spectrum has a single spectral index of $n \sim -4.5$ throughout the measured wavenumber range, which is equivalent to an electric field spectral index of -2.5. The potential and the density spectral indices differ by 2 in the long-wavelength region ($k_\theta \rho_i < 0.3$) and are equal in the short-wavelength region ($k_\theta \rho_i \geq 0.3$). These laboratory observations are similar to *in situ* measurements of ESF[8]. The observed spectral indices in our experiment for $k_\theta \rho_i < 0.3$ are consistent with the relation between density and potential fluctuations for the case of RT instability. It is by now well established theoretically that RT instability mechanism plays a crucial role in the generation of k^{-2}-spectrum in the long-wavelength regime[13]. A comparison of the observed experimental spectra with *in situ* measurements and with predictions of the nonlinear theories indicates that the shallower $k^{-2.5}$ spectra for density and electric field might result from RT instability mechanism operating in the long-wavelength regime.

The spectrum shown in Figure 3 exhibits a spectral index of about -4.5 for both density and potential fluctuations for $k_\theta \rho_i > 0.3$, suggesting that the Boltzmann relation is obeyed in this scalelength regime. Experimental observations of short-wavelength fluctuations ($k\rho_i \geq 1$) in density and potential in the equatorial ESF[14] exhibit similar characteristics. A two-step process[15] has been proposed for the generation of short-wavelength instability in the equatorial spread-F invoking the generation of large-scale irregularities by the RT process, followed by excitation of drift waves on gradients associated with the primary process. Using the gradients associated with long wavelengths, we find that the growth rate of drift waves exceeds that of RT instability in the short-wavelength regime. This, together with the similarity between the observed spectra and the *in situ* measurements in the ESF, points to drift waves growing through a two-step process as a possible cause for the short-wavelength instability observed in our experiment. Theoretical calculations[16], numerical simulations[17] and laboratory experiments[18] predict a one-dimensional spectral form with index in the range of

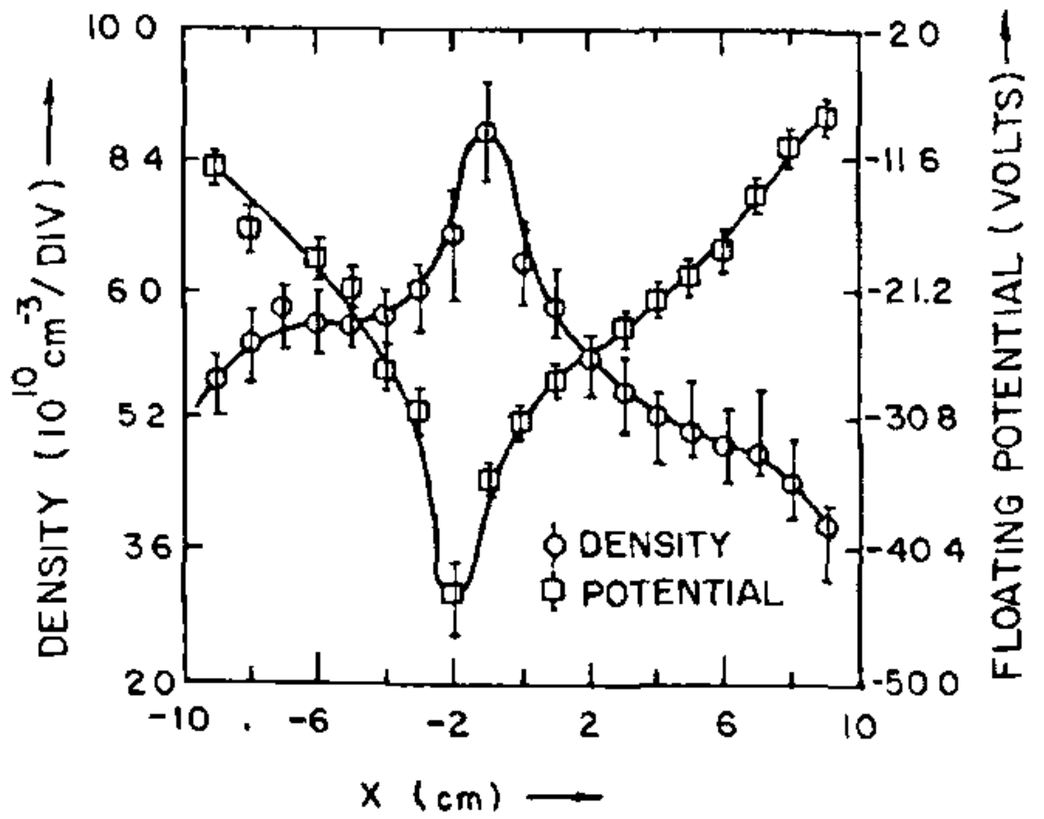

Figure 4. Variation of the plasma density and the floating potential as a function of the distance x from the minor axis at one toroidal location in type-II experiments

-4.5 to -5 for drift waves. All these observations are sufficient to conclude that the steeper slope ($n \sim -4.5$) observed in our experiment at shorter wavelengths is due to drift wave turbulence.

Type-II experiments

In these experiments the filament is located at the centre of the machine cross-section, enabling us to produce profiles that are peaked near the centre. The density and floating potential profiles, measured at 1 kG of toroidal magnetic field value (shown in Figure 4), indicate that gravity is antiparallel to ∇n between the positions $x = -1.0$ cm and $x = 9$ cm (corresponding to region I of the F-region) and parallel to ∇n between the positions $x = -2.0$ cm and $x = -9$ cm (similar to region II of the F-region). The distance x refers to the distance from the minor axis and is defined in Figure 1. The electron temperature in the system varies from 5 to 19 eV. The plasma produced satisfies the condition of collisionality of the F-region ($\nu_{in}/\Omega_i \ll 1$ and $\nu_{en}/\Omega_e \ll 1$). The rms value of the fluctuations is $\tilde{n}_{rms}/n_0 \sim 20$–$40\%$, with $\tilde{n}/n_0 \simeq e\tilde{\phi}/T_e$.

In region I the gravity effect is relatively strong at $\nu_{in}/\Omega_i \ll 1$. The local wavenumber spectra of density and potential fluctuations are shown in Figure 5 for regions I and II. The density spectra have clearly two slopes in both the regions, with spectral indices $n \sim -2.5$ for $k_\theta \rho_i \leq 0.3$ and $n \simeq -4.5$ for $k_\theta \rho_i \geq 0.3$. The potential spectra have only one slope with spectral index $n \simeq -4.5$ in both region I and region II. We also observe that the difference between density and potential spectral indices is ~ 2 for $k_\theta \rho_i \sim 0.3$ whereas it is zero for $k_\theta \rho_i \geq 0.3$. The waves have long wavelengths in the radial and

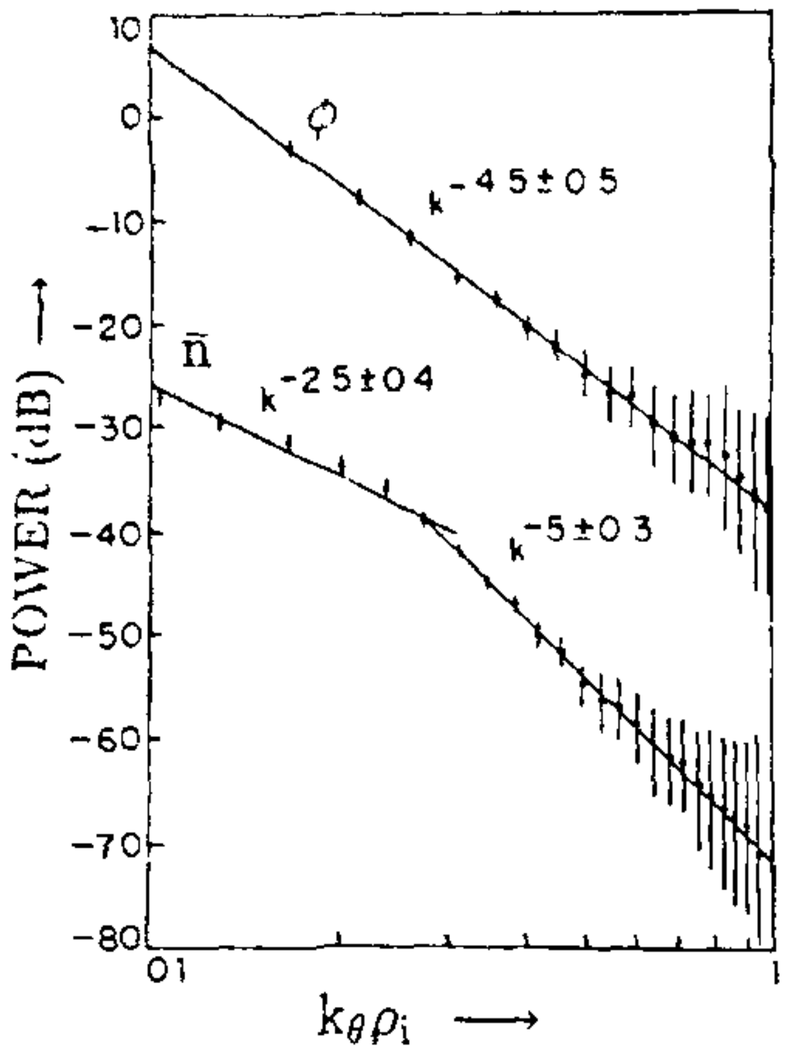

Figure 5. Wavenumber spectra for the density and the potential *a*, in region-I. *b*, in region-II for type-II experiments

parallel directions, propagating mainly in the azimuthal direction, similar to the observations in type-I experiments. The observed fluctuation characteristics in both the regions are similar to those observed in type-I experiments. However, region II is, in principle, stable against RT instability. The numerical simulation studies[19] have shown that the irregularities first excited in the region of the plasma where g is antiparallel to ∇n, by RT instability, then bubble to the top side of the F-region density peak by $\mathbf{E} \times \mathbf{B}$ polarization motion. *In situ* observations[14] have confirmed similar spectra of density fluctuations above the F-region peak density. We have also observed similar spectra in regions I and II. However, we observe the fluctuations simultaneously in both the regions. A lag in the onset of these fluctuations in region II, as found in numerical simulation studies or *in situ* experiments, is not possible to observe in our case due to the large growth rate and $\mathbf{E}_0 \times \mathbf{B}$ motion of the instabilities and geometrical constraints on the system.

Effect of collisionality on the spectra

In our observations the shallower slope in the density spectrum for $k_\theta \rho_i < 0.3$ (Figure 3) may be due to the stabilization of RT instability by the finite Larmour radius effect[20]. The shallower part of the spectrum extends up to short perpendicular wavelengths and is an indication of finite ν_{in} and ν_{ii} collisions. In order to see these effects more explicitly, we varied the neutral gas (Ar) pressure from 10^{-4} to 4×10^{-3} torr and the magnetic field strength from 400 G to 1 kG, providing data over a ν_{in}/Ω_i range of 0.04–1.0. Under these operating conditions, $\nu_{en}/\Omega_e \ll 1$ is always satisfied and hence the electrons are magnetized. The density and potential fluctuations observed under these conditions are found to be turbulent. The variation of the spectral index with ν_{in}/Ω_i is shown in Figure 6 for type-I experiment. The density fluctuations exhibit two slopes for ν_{in}/Ω_i in the range 0.04–0.2, whereas the potential spectrum exhibits a single slope. The spectral relation

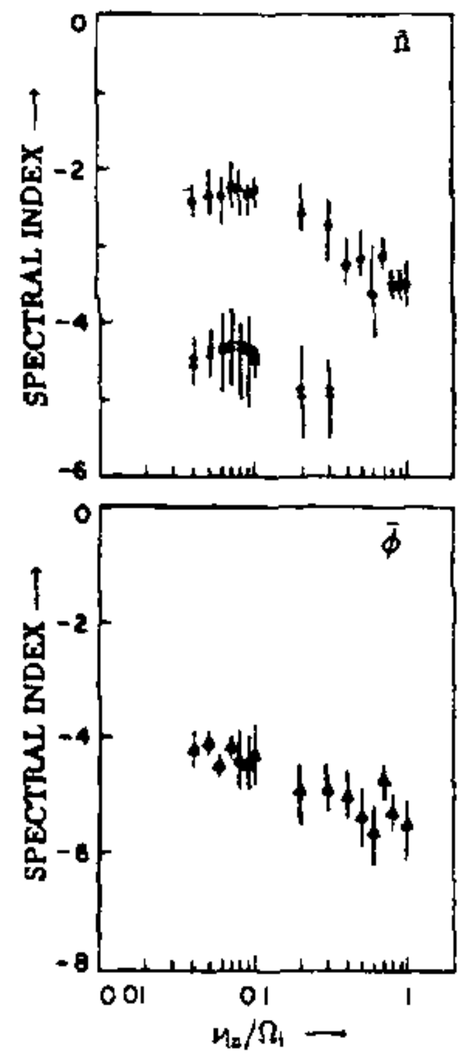

Figure 6. Spectral indices for density and potential spectra at various collision frequencies in type-I experiments

for density and potential for the case of RT and drift wave instabilities are satisfied for the above range of ν_{in}/Ω_i. As ν_{in}/Ω_i is increased further, the density spectrum loses the dual-slope character and starts exhibiting a single index for the entire k-range.

The plasma with $\nu_{in}/\Omega_i > 0.2$ deviates from the F-region plasma. In this regime the ions are highly collisional and the gravitational effect decreases, i.e. the value of E_0/B becomes comparable to g/ν_{in}. The spectral index of density fluctuations approaches −3.5, whereas the spectral index of potential fluctuations approaches ~ −5.5. At these values the observed spectral indices correspond neither to RT instability nor to drift instability. The growth rates of RT instability[20] and drift instability[18] decrease with increase in ν_{in}/Ω_i. When $\nu_{in}/\Omega_i \geq 1$, an altogether different instability, in which the difference in the spectral indices of density and potential is about 2, emerges. The observations in the present case indicate a transition to a collision-dominated instability, viz. the gradient drift instability or the cross-field instability[5] (an analog of RT instability in the collisional regime), observed in equatorial electrojet region[2, 3] and related laboratory experiments[21]. Detailed observations of this instability in our device are presented in the next section. Similar results are obtained in type-II experiments with variation in neutral gas pressure.

Experiments related to E-region instabilities

A number of laboratory experiments[21] have confirmed the excitation of Farely–Buneman and cross-field instabilities under conditions similar to those existing in equatorial electrojet. These instabilities in equatorial electrojet develop strongly unstable fluctuations. The fully developed turbulence has been investigated in detail both *theoretically*[22] *and by numerical simulation*[23]. Laboratory experiments on the turbulent state are, however, scarce. In most of these experiments[21] frequency spectra of the coherent modes have been measured. From the viewpoint of comparison with theory and *in situ* measurements, the measurements of the wavenumber spectra are desirable. In what follows, we report the results on the k-spectrum of the turbulent density and potential fluctuations arising from cross-*field instability in the collisional regime*. The experiments[24] were carried out in argon plasma at a pressure of 3 m torr and at an applied magnetic field of 200 G. Under these conditions, the electrons are magnetized ($\nu_{en}/\Omega_e \ll 1$) and the ions are unmagnetized ($\nu_{in}/\Omega_i \leq 1$). Typical density and the potential profiles measured in the radial direction in a plane perpendicular to the magnetic field are similar to those shown in Figure 2. The peak plasma density is $\approx 10^{11}$ cm^{-3}, the electron temperature $T_e \approx 4$ eV and the ion temperature $T_i \approx 0.20$ eV. The density gradient scale size $L_n = (\nabla n/n)^{-1} \approx 18$ cm at the radial position, where measurements are made. The potential profiles indicate the presence of an electric field parallel to ∇n, and $\mathbf{g}$ antiparallel to ∇n. The plasma thus satisfies conditions for the existence of collisional gradient drift or cross-field instability and RT instability. At these operating parameters, strong density and potential fluctuations are observed. The density fluctuations at radial position of 6 cm for frequencies below 25 kHz have an rms amplitude of ≈ 40%, with $\langle e\tilde{\phi}/T_e \rangle_{rms} = \langle \tilde{n}/n \rangle_{rms}$. The observations indicate that the fluctuations have a frequency $\omega < kC_s$, where k is the wavenumber and C_s is the ion-acoustic speed. Thus, the conditions for the growth of Farley–Buneman instability are not satisfied. The measurements of the parallel ($k_\parallel$), the radial (k_r), and the azimuthal (k_θ) wavenumbers indicate that the waves propagate mainly in the azimuthal direction, with $k_\parallel \ll k_\theta$ and $k_r \sim k_\theta$. Analysis of the linear, low-frequency ($\omega < \Omega_i$) growth rate[25] indicates that the growth term due to crossfield instability dominates over the contributions from the curvature of the magnetic field.

The auto-power spectrum of the fluctuations indicates that the fluctuations are turbulent in nature, with no prominent peaks in the spectrum. The wavenumber spectra for density and potential fluctuations are shown in Figure 7. The solid lines are the least square fits of the data to a power law, ($S(k) \propto k^n$). The spectra are one-dimensional and correspond to azimuthal wavenumber k_θ. Both density and potential spectra are flat at smaller wavenumbers ($k_\theta \rho_i < 0.2$), with spectral index ≈ −1.0 for density fluctuations. The spectra become steeper for larger wavenumbers. The wavenumber spectrum has a

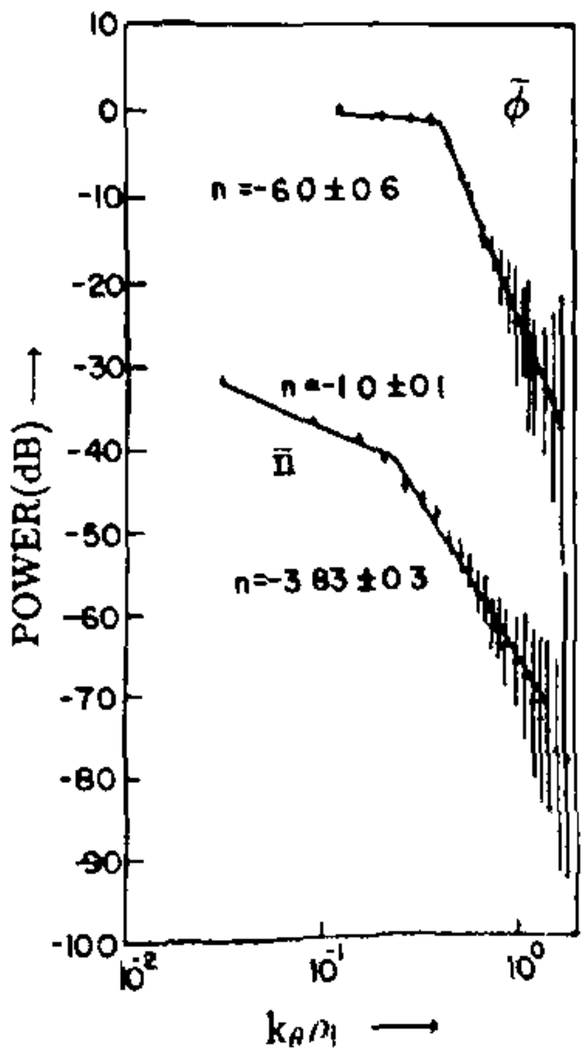

Figure 7. Wavenumber spectra for density and potential fluctuations in the collision-dominated regime

spectral index of -3.8 ± 0.5 and -6.0 ± 0.6 for density and potential fluctuations, respectively, for $k_\theta \rho_i \geq 0.2$ wavenumber range. The k-spectra indicate the presence of fluctuations for k_θ up to 6 cm^{-1}. The linear theory, however, predicts that for $k_\theta > 0.5$ cm^{-1} the fluctuations should be damped. The large-k, shorter-wavelength instabilities, which are linearly damped, could be excited by a two-step mechanism[22] from the large-amplitude longer-wavelength waves in our experiment. The observed spectral indices are similar to those obtained in earlier experiments[21], where the spectral indices were estimated from the observed multimode frequency spectra and conversion to wavenumber spectra using the observed dispersion relation. The present observations thus confirm these spectral characteristics in the turbulent regime. Mikkelsen and Pécseli[18] obtained a spectral index of –5.0 for potential fluctuations associated with cross-field instability in the high-frequency regime, which is similar to, but smaller than, the k-spectrum index obtained in the present experiments on low-frequency cross-field turbulence. The spectral index for density fluctuations observed in our experiments is in close agreement with *in situ* measurements[3].

Unified theories[13] for electrojet instabilities and long-wavelength strongly turbulent fluctuations in the E- and the F-region[2] predict a one-dimensional power law of the form $k^{-5/3}$. The two-dimensional simulation studies of cross-field instabilities[23] predict a spectral index between -3 and -4 for density fluctuations (which should correspond to an index of -2 to -3 for the one-dimensional spectrum). The present observations thus indicate k-spectra steeper than those obtained in these numerical simulations. Numerical simulations[26] of large-scale irregularities (perturbation scale sizes of the same order as the equilibrium gradient scale length) yield one-dimensional integrated density and electric field power spectra with power index ranging from -2.5 to -1.2. The range of k values for which the present observations give a flatter ($n = -1.0$) spectrum corresponds to wavelengths of the order of the gradient scale lengths in our system.

Conclusions

Many features of the observed spectral characteristics of the ionospheric instabilities have been reproduced in laboratory plasma experiments. The observations indicate an important role of the plasma instabilities in generating ionospheric irregularities.

1. Ossakow, S L, *Rev. Geophys. Space Phys*, 1979, **17**, 521–533, Fejer, B G and Kelley, M. C., *Rev Geophys Space Phys*, 1980, **18**, 401, and the references therein
2 Farley, D T, *Rev Geophys Space Phys*, 1974, **12**, 285–289, and the references therein
3 Prakash, S, Gupta, S P. and Subbararya, B H., *Radio Sci.*, 1969, **4**, 791–796, Prakash, S, Gupta, S. P. and Subbararya, B H, *Nature Phys Sci*, 1971, **230**, 170–171; Prakash, S, Gupta, S P, Subbararya, B H, Sinha, H S S and Jain, C. L, First Lloyd Berkner Symposium, AGU, Dallas, Texas, 1973
4 Farley, D T., *J Geophys Res*, 1963, **68**, 6083, Bunemann, O, *Phys Rev Lett*, 1963, **10**, 285.
5. Rogister, A and D'Angelo, N, *J Geophys Res*, 1970, **75**, 3879–3887; Schmidt, M. J and Gary, S P., *J Geophys Res*, 1973, **78**, 8261–8265.
6 Kelley, M C. and McClure, J P, *J Atmos Terr Phys*, 1981, **43**, 427–435, Chandra, H, *Ind J Radio Space Phys*, 1990, **19**, 215–224
7. Ossakow, S L, *J Atmos Terr Phys*, 1981, **43**, 437–452, and the references therein
8 LaBelle, J and Kelley, M C, *J Geophys Res*, 1986, **91**, 5504–5512
9 Prasad, G, Bora, D and Saxena, Y C, *Geophys Res Lett*, 1992, **19**, 241–244, Prasad, G, Bora, D and Saxena, Y C, *Geophys Res. Lett*, 1992, **19**, 245–247, Prasad, G, Bora, D, Saxena, Y. C. and Verma, S. D, Insitute for Plasma Research Report IPR/RR-73/92, 1992.
10 Bora, D, *Phys. Lett*, 1989, **139A**, 308–312
11 Smith, D E., Powers, E. J and Caldwell, G. C., *IEEE Trans Plasma Sci*, 1974, **PS-2**, 261–272
12. Beall, J M, Kim, Y C and Powers, E J, *J Appl Phys*, 1982, **53**, 3933–3940
13 Balsley, B B, Haerendal, G and Greenwald, R A, *J. Geophys Res*, 1972, **77**, 5625–5630; Costa, E and Kelley, M C, *J Geophys Res*, 1978, **83**, 4359–4372; Sudan, R N. and Keskinen, M J, *J Geophys Res.*, 1984, **89**, 9840–9845
14 Singh, M and Szuszczewicz, E. P., *J Geophys Res*, 1984, **89**, 2313–2323, Kelley, M C, Pfaff, R P, Baker, K. D, Ulwick, J C, Livingstone, R, Rino, C. L and Tsunoda, R, *J Geophys Res*, 1982, **87**, 1575–1583, Kelley, M C., Livingstone, R, Rino, C L and Tsunoda, R, *J Geophys Res*, 1982, **87**, 5217–5221
15 Chaturvedi, P K and Kaw, P K, *J Geophys Res*, 1976, **81**, 3257–3260
16 Hasegawa, A. and Mima, K, *Phys Fluids*, 1978, **21**, 87–94, Fype, D and Montgomery, D, *Phys Fluids*, 1979, **22**, 246–250, Tchen, C M, Pécseli, H L and Larsen, S E, *Plasma Phys*, 1980, **22**, 817
17 Hasegawa, A Maclennan, C. G and Kodama, Y, *Phys Fluids*, 1979, **22**, 2122–2130
18 Pécseli, H L., Mikkelsen, T and Larsen, S E, *Plasma Phys*, 1983, **25**, 1173–1197, Mikkelesen, T and Pécseli, H L, *Phys Lett*, **77A**, 159–162, Chen, F F, *Phys Rev Lett*, 1965, **15**, 381–385
19 Scannanpieco, A. J and Ossakow, S L., *J Geophys Res*, 1976, **81**, 6037–6045
20 Rosenbluth, M. N, *Microinstabilities in Plasma*, IAEA, Vienna, 1965, Hudson, M K and Kennel, C. F, *J Geophys Res*, 1975, **80**, 4581–4586
21. Saxena, Y. C, in *Relation between Laboratory and Space Plasmas* (ed Kikuchi, K), D. Riedel, Holland, 1981, pp 171–185, and the references therein
22 Ott, E. and Farley, D T., *J. Geophys Res*, 1974, **79**, 2465–2480, Sudan, R. N. and Keskinen, M J, *J Geophys Res*, 1977, **38**, 966–970
23. McDonald, B E, Coffey, T P, Ossakow, S L. and Sudan, R N, *J Geophys. Res*, 1974, **79**, 2551–2562, Sato, T and Okuda, T, *J Geophys Res*, 1976, **81**, 3248–3251, Tsuoda, T and Sato, T, *Phys. Fluids*, 1968, **11**, 676–683
24 Prasad, G, Bora, D. and Saxena, Y. C, Institute for Plasma Research Report IPR/RR-84/92, 1992
25. Mahajan, Sangeeta, Singh, R and Kaw, P K, Private communication.
26 Ronchi, C, Sudan, R N and Farley, D T, *J Geophys Res*, 1991, **96**, 21283–21295

ACKNOWLEDGEMENT The work reported here was carried out in collaboration with Mr Ganesh Prasad and Dr D Bora and forms a part of the Ph D thesis of Mr Ganesh Prasad

Received 8 January 1993, revised accepted 14 September 1993